

Article

Study on the Mechanical Performance of RC Beams under Load Reinforced by a Thin Layer of Reactive Powder Concrete on Four Sides

Wei Liao *, Weijun Yang and Jianyu Yang

School of Civil Engineering, Changsha University of Science & Technology, Changsha 410114, China; yyyaozhijian@163.com (W.Y.); jianyuy@csust.edu.cn (J.Y.)

* Correspondence: 13873151088@163.com; Tel.: +86-13873151088

Abstract: To repair reinforced concrete beams efficiently in a limited building space, the four-sided application of a reinforcing thin layer of reactive powder concrete (“RPCTL”) was proposed to improve the bending capacity of the members. Static flexural tests of one comparison beam and five reinforced beams were completed on a four-point centralized loading device. Changes in deflection, cracks, stresses, and damage characteristics of the specimens were measured under various levels of loading. The test results showed that the damage patterns of the reinforced specimens were dominated by the yielding of longitudinal tensile reinforcement at the bottoms of the beams and the crushing of the cementitious material in the top compression zones of the beams. The cracking load greatly increased by 1.42 to 7.12 times, and the ultimate bearing capacity increased by 0.29 to 1.41 times. The distribution characteristics and dynamic changes in the displacement, stress, and damage of the specimens were dynamically simulated by finite element software. The effects of reinforcement and initial load-holding level on the reinforcement effect were investigated. A bending capacity calculation formula for RPCTL reinforcement technology is proposed that aligns with the test results and can provide a reference for the design of RPCTL reinforcement.

Keywords: reactive powder concrete; thin layer; reinforcement; RC beams



Citation: Liao, W.; Yang, W.; Yang, J. Study on the Mechanical Performance of RC Beams under Load Reinforced by a Thin Layer of Reactive Powder Concrete on Four Sides. *Buildings* **2024**, *14*, 1451. <https://doi.org/10.3390/buildings14051451>

Academic Editor: Nerio Tullini

Received: 18 April 2024

Revised: 7 May 2024

Accepted: 12 May 2024

Published: 16 May 2024



Copyright: © 2024 by the authors. Licensee MDPI, Basel, Switzerland. This article is an open access article distributed under the terms and conditions of the Creative Commons Attribution (CC BY) license (<https://creativecommons.org/licenses/by/4.0/>).

1. Introduction

With the continued emergence of new materials and technologies, an increasing number of reinforcement methods are being proposed for reinforced concrete members, most commonly for the reinforcement of bending members. Damage of reinforced concrete beams is common to see when a member cracks during an earthquake, impact and explosion, or the bearing capacity is weakened due to design or construction reasons. As such, reinforcement methods which can provide great bearing capacity and protection are very important for structural safety. The traditional concrete beam reinforcement technique is to paste a new laminated surface layer or a single tensile material at the bottom of the beam to increase the load-carrying capacity and stiffness by enhancing the amount of reinforcement in the original member.

Single-point concentrated loading tests were performed by Azeez A. A. [1] on deep beams reinforced with carbon fiber tensile reinforcement and reactive powder concrete, and the results showed that the cracks on the surfaces of the deep beams reinforced with reactive powder concrete were effectively suppressed. Zhelyazov T. [2] tested the flexural reinforcement of reinforced concrete beams in coastal areas using basalt with basalt fiber-reinforced polymer (BFRPS), and the results showed that, although the modulus of elasticity of BFRP reinforcement was lower than that of structural steel, the increase in load-carrying capacity increased with pretensioning. Codina A. [3] analyzed the mechanical behavior of reinforcement damage caused by debonding failure at the bottom mid-span crack area of beams based on four-point bending tests and the model evaluation of three

FRP- and CFRP-reinforced concrete beams. Gedik Y.H. [4] installed longitudinal carbon fiber-reinforced polymer tendons on the surface of stone beams and constructed a total of 11 stone beams with different reinforcement and prestressing levels for testing their bending performance. The results showed that the composite beams configured with CFRP tendons with or without applied prestressing exhibited ductile failure, with significant deflection and multiple cracks after damage.

Other researchers have applied bamboo and wood materials [5], recycled metals, and composite fiber alternative materials as reinforcement. However, these tensile materials differ greatly from the deformation modulus of concrete; there is an obvious stress hysteresis problem [6]. In addition, these techniques involve extracorporeal reinforcement at the bottom of concrete beams, but as this type of flexural reinforcement transmits forces in a single direction, resistance to peeling measures is limited [7]. Especially in members with large cross-sections, even if end anchors or reinforcing hoops are provided, it is difficult to allow the reinforcement layer and the original member to fully co-stress [8].

Compared to the traditional concrete beam reinforcement techniques, some researchers tend to reinforce the concrete beams around the perimeter with a composite surface layer consisting of steel reinforcement mesh and recycled concrete [9], high-performance mortar, and activated powder concrete, which not only eliminates the stress difference to a large extent and has better compatibility with the member concrete, but also provides better protection to the internal steel reinforcement [10]. Among them, RPC is gaining attention for its excellent performance in the application of reinforcement works.

Zheng Wang [11] conducted an experiment to study on the influence of the steel fiber types on RPC performance. It showed that appropriate ratio of length to diameter will give full play to the tensile effect of steel fiber in the material and ensure it is evenly distributed. Chuanlin Wang [12] studied the influence of three types of open and three different shapes of closed steel fibers on the working and mechanical performance of RPC, showing that the open steel fibers enhance the mechanical performance of RPC via their anchoring performance while the closed steel fibers work by confining the concrete. Qin Rong [13] studied the dynamic response of RPC columns based on the equivalent single-degree-of-freedom method and P-I curve and obtained the effect of five parameters on the degree of damage under different blast loadings, which provides a valuable reference for the dynamic response of RPC members. Mo Liu [14] studied the microscopic morphology and structure of basalt fiber reactive powder concrete (BFRPC), and established the strength calculation formula of BFRPC. Shatha D. Mohammed [15] provides an experimental analysis of the structural behaviors of reinforced RPC beams under harmonic loads, in which the outcomes proved the positive effect of adding steel fibers on the dynamic response under the effect of harmonic loading in RPC. Jie Xiao [16] carried out a study to solve the problem of steel bars in ordinary reinforced concrete structures by replacing steel bars with basalt fiber-reinforced polymer bars and replacing ordinary concrete with reactive powder concrete, considering the law of bond strength and protective layer thickness.

Nowadays, many researchers have started to use activated powder concrete with steel reinforcement to improve the load-carrying capacity and stiffness of flexural members.

Lee Ming-Gin [17] used RPC to reinforce concrete beams at the bottom. The results showed that the effect of using RPC material with a thickness of 20 mm and a steel fiber content of 1.0% is approximately equivalent to the reinforcement effect of three layers of carbon fiber-reinforced polymer (CFRP). Yang Yang [18] proposed a method for reinforcing beams by adding layers of RPC at the bottom tension zone and top compression zone of the beams. The bending test of six specimens was conducted to analyze the effects of area substitution ratio and reinforcement ratio of the composite layers. Yang Kejia [19] controlled the distribution of steel fibers in RPC through a magnetic field. Four-point bending tests showed that the flexural capacity of activated powdered concrete flexural specimens after the directional distribution of steel fibers increased by 72.4–149.5%.

Yang Zhang studied the flexural strength and stiffness of reinforced concrete beams reinforced with layered RPC added to the bottom [20] and compared the differences in the

damage patterns of the new prestressing and normal reinforcement in the reinforcement layers [21]. Bahraq A A [22] conducted an experimental study and numerical analysis of the stress performance of reinforced concrete beams reinforced with ultrahigh-performance fiber-reinforced concrete. Deng Mingke [23] compared the tensile ductility of concrete beams subjected to bending repaired with HDC and RPC surface layer. Farzad M. [24] tested the interfacial properties between UHPC and reinforced concrete elements and developed a mathematical model to predict the reinforcing performance of the overlay, and this provided a reference for the transmission mechanism of the reinforcement technology using a surface layer of RPC. In comparison, Zhu Zhiwen [25] investigated the flexural behavior of ordinary beams and gap beams reinforced with RPC under long-term sustained loads for 23.6 years. The displacement ductility of the strengthened beams decreased by 82–94%. Qin Fengjiang [26] reported that the energy dissipation capacity, cracking resistance, and cracking load of ECC-enhanced specimens greatly improved with increasing reinforcement thickness.

However, these aforementioned studies on activated PCR technology for various composite surfaces reinforcing concrete beams are still dominated by beam-bottom laminations or three-sided U-shaped reinforcement, and the current research and engineering applications are based on lower-strength grades of concrete or mortar as a reinforcement material, where the reinforcement layer is very thick and the use of space is limited. In other fiber composite materials, the strain hysteresis is too great [8], and, for flexural reinforcement layers subjected to a single direction of force transfer, resistance to peeling measures is limited [7], especially in larger members where it is difficult to set the anchors, reinforcing hoops, and other measures necessary to bond the reinforcement layer and the original member to withstand the full synergistic force. Few studies have been conducted on the reinforcement of beams by four-surface applications of thin layers, and there are few reports on the use of reinforced reactive powder concrete as a material for reinforcement.

Based on the above research, this paper proposes a four-sided application of a reinforcing thin layer of reactive powder concrete (RPCTL). There are two main features of the reinforcement effect of RPCTL. First, the longitudinal reinforcement at the bottom of the beam is directly subjected to tensile force, and the tensile load capacity of the bending zone is improved by increasing the amount of reinforcement. Second, the deformation of the original members can be inhibited by restraining the concrete in the core area, thus improving the flexural stiffness [27]. Compared with three-sided applications, four-sided RPCTL reinforcement has a stronger restraining effect on the core zone, and the stress hysteresis effect is weaker than that of fiber composites or prestressing tendon reinforcements. The RPCTL has a smaller thickness, is lightweight and has a high strength, and provides greater reinforcement efficiency.

RPC has good bonding ability with concrete, and steel mesh in a thin layer enhances the integrity and mechanical performance. In addition to the RPC in contact with concrete, this composite structural layer is connected to the original structure by pins. The RPC thin layers do not obstruct interior space, it can be poured after formwork is installed, or spread on the surface of concrete directly, which is proven to be a very convenient method for construction.

To investigate the bending performance of reinforced concrete beams reinforced by RPCTL technology on all sides, this paper designs six-foot beams to carry out static bending loading tests to study the effects of the thickness of the viscous reinforcement layer and the initial load-holding level on the bending performance of the reinforced beams and proposes a method for calculating the bending capacity of RPCTL technology.

2. Test Design

2.1. Specimen Design

Six full-scale reinforced concrete test beams were designed with specimen lengths of 4200 mm, cross-sectional dimensions of 200 × 400 mm, and the same reinforcement

skeleton configuration. One specimen, RCFB1, was used as a comparison beam, and the other five were reinforced with RPCTL (Figures 1 and 2).

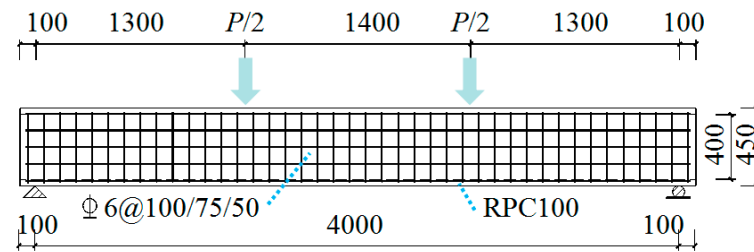


Figure 1. Structure of the RPCTL.

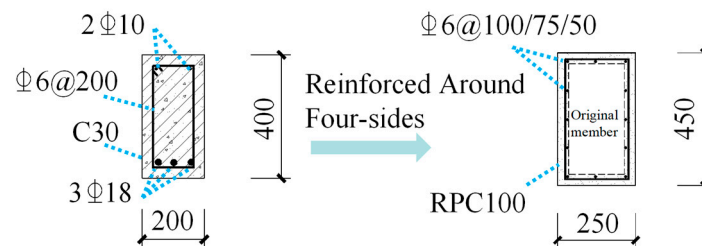


Figure 2. Section of specimens.

The initial load level of SRFB2 was set to 0%. The reinforcement was carried out directly after the fabrication and curing of the original members, and the bending test was carried out after the thin layer of reactive powder concrete reached the design strength. SRFB3, SRFB4, and SRFB5 were load-holding reinforced after applying up to 50% of the computed ultimate load capacity of the original member. A secondary force test was carried out after the thin layer of reactive powder concrete reached the design strength. The initial load level of SRFB6 was further increased to 80% before the load-holding reinforcement. The parameters of each specimen are shown in Table 1.

Table 1. Specimen parameters (mm).

Specimen	Thickness of RPCTL	Reinforcement Mesh in RPCTL	Initial Load Level
RCFB1	/	/	/
SRFB2	25	Φ6@50	0
SRFB3	25	Φ6@100	50%
SRFB4	25	Φ6@75	50%
SRFB5	25	Φ6@50	50%
SRFB6	25	Φ6@50	80%

2.2. Material Properties

The test beams were cast in C30 concrete with 18 mm diameter longitudinal bars and 6 mm diameter hoop bars in the reinforcement skeleton. The reinforced thin layer was made of reactive powder concrete with a strength class of RPC100 with an optimized steel fiber volume mix of 2% [28], and the longitudinal and transverse reinforcement mesh configured in the reinforced layer was made of 6 mm diameter steel bars. The material properties are shown in Tables 2–6.

Table 2. Composition of the reactive powder concrete ratio (kg/m³).

Cement	Silica Fume	Quartz Sand 0.5–1 mm	Quartz Sand 0.2–5 mm	Polycarboxylic Acid-Based High-Efficiency Water Reducing Agent	Water	Steel Fiber
1000	250	0	1000	30	200	256

Table 3. Composition of the concrete mix ratio (kg).

Water	Cement	Sand	Gravel
175	416	512	1252

Table 4. Mechanical properties of the concrete.

Grade of Concrete	f_c /MPa	f_t /MPa	E_c /GPa
C30	35.5	2.04	3.0

Table 5. Mechanical properties of the reactive powder concrete.

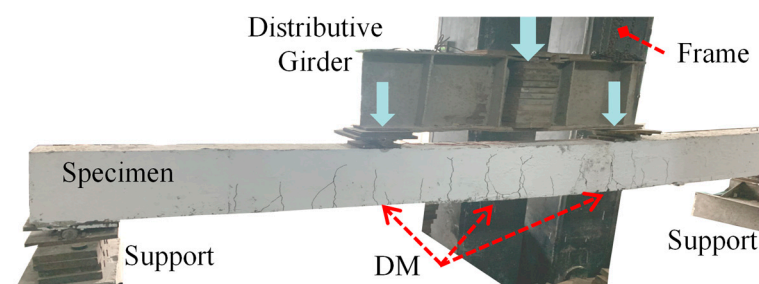
Grade of RPC	f_{rc} /MPa	f_{rt} /MPa	E_{rc} /GPa
RPC100	115.2	10.7	43.0

Table 6. Mechanical properties of the reinforcing steel.

Grade of Reinforcement Mesh	Diameter/mm	f_y /MPa	E_s /GPa
HRB335	6	346	215
HRB335	10	339	203
HRB335	18	355	201
HRB400	6	431	208

2.3. Loading Program

The original member was supported on hinged bearings at both ends, with a clear span of 4000 mm. The specimen was placed under a reaction frame, and a hydraulic jack was used to apply the force and loaded at two points in the middle of the top of the beam using a section distribution beam (Figures 3 and 4). Displacement gauges were arranged at the bottom of the beam in the loaded mid-span section to read the deflection changes, and the loading was controlled by a hydraulic servo system to observe the cracks and deflection changes after stabilization under each level of loading. For specimens subjected to secondary loading, steel plates and wedges were used to tighten the gap between the reaction frame and the distributing beam immediately after the initial load was applied, thus maintaining the initial load level for subsequent reinforcement of the test beams.

**Figure 3.** The loading device.

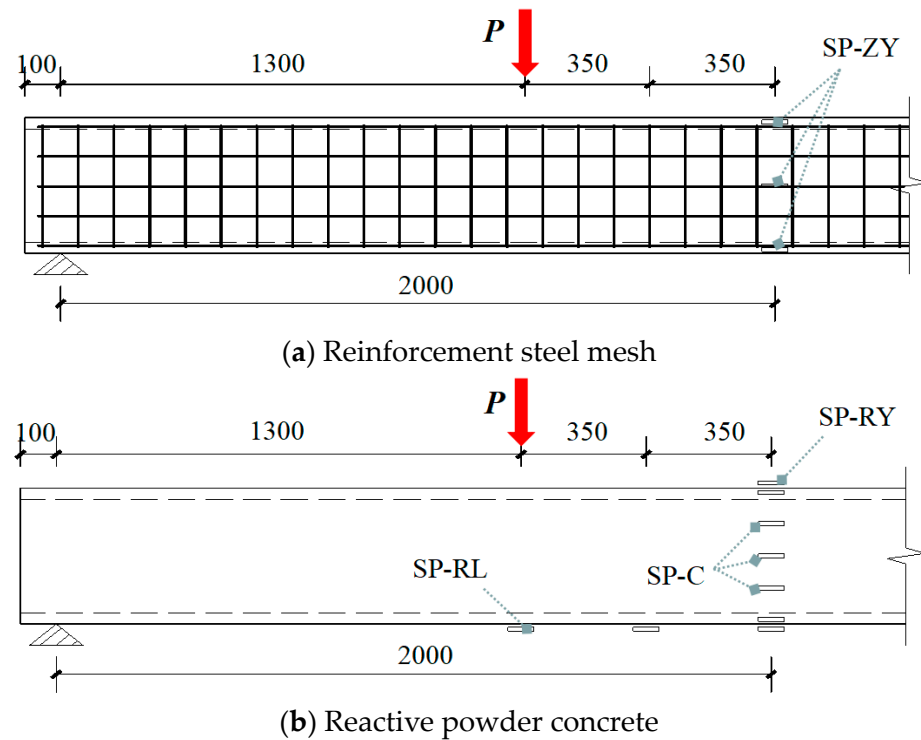


Figure 4. Strain measurement points of the RPCTL in the mid-span section.

3. Test Results and Analysis

3.1. Experimental Phenomena

The bending damage process of each test beam subjected to secondary force can be roughly divided into three stages: (1) The early loading stage is the elastic stage, where the displacement is linearly related to the load change and the initial crack is not obvious. (2) After the first microcrack appears in the reinforcement layer at the bottom of the beam in the purely curved section, the test specimen enters the elastic–plastic deformation stage, where the slope of the load–displacement curve decreases slightly, several parallel cracks appear one after another, and the first crack extends upward and widens to form the main crack. The first crack extends upward and widens to form the main crack. With increasing load, the distribution of cracks on the lateral side of the beam gradually increases, and adjacent vertical cracks gradually bifurcate and connect diagonally, forming a decentralized crack network. (3) With further extension and intensification of the main crack, the test beam reaches the damage stage, and the deflection and deformation of the specimen increase rapidly. Under the load condition, the longitudinal bars at the bottom of the beam of the original member are the first to reach yield, the stress is rapidly transferred to the longitudinal bars in the reinforced thin layer at the bottom of the beam and continues to be transferred as the former yields, and the longitudinal bars in the reinforced layer at the side of the beam also reach the limit state from the bottom up. As the original longitudinal bars in the bottom of the beam and the longitudinal bars in the reinforced layer yield and pull out successively (Figure 5), the concrete at the top of the beam and the reinforced layer of reactive powder concrete between the two loading points are locally crushed. After the damage, the cracks on the side of the beam are scattered and dense, while the main crack openings are obvious, and part of the longitudinal bars in the side reinforcement layer yield and deform. Pulled-out and deformed steel fibers from the reinforcement material are visible at the collapse sites and crack openings (Figure 6).

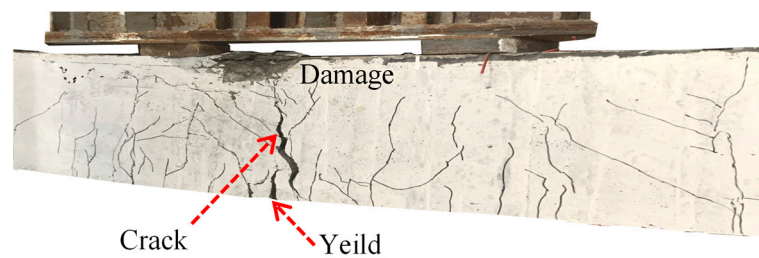


Figure 5. Local failure of the reinforced specimen.

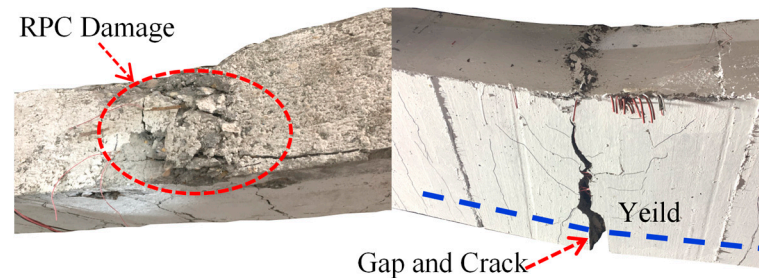


Figure 6. Typical failure in the mid-span section.

3.2. Test Results

The test results of each specimen are shown in Table 7 and indicate that the cracking load and ultimate load of the concrete beams significantly increased after thin-layer reinforcement with reactive powder concrete.

Table 7. Test results.

Specimen	Cracking Load (kN)	Ultimate Load (kN)	Maximum Deflection (mm)
RCFB1	15.8	143.3	103.2
SRFB2	38.3	345.3	48.1
SRFB3	97.2	243.5	53.4
SRFB4	102.3	269.5	61.5
SRFB5	112.9	311.5	42.0
SRFB6	128.3	185.3	33.6

As shown in Figure 7, for the load–deflection curves, the slopes of the load curves in the elastic phase of the reinforced specimens increased to different degrees, indicating that the new steel reinforcement mesh and the reactive powder concrete material in the reinforced thin layer worked well together with the original members. The first inflection point of the slope of the curve appeared after the second stress cracking, the initial crack to the reactive powder concrete of the reinforced thin layer at the bottom of the beam stopped advancing, and the bridging effect of the steel fibers subsequently failed [29]. Afterward, the longitudinal reinforcement stresses in the reinforced layer continued to increase, the original longitudinal reinforcement and the newly added longitudinal reinforcement at the bottom of the beam reached one region after another, and the slope of the curve gradually decreased. When approaching the ultimate bearing capacity, the specimens with different initial load levels successively reached the yielding state of most longitudinal bars, the second inflection point appeared in the curve, the slope became significantly smaller or even close to the level, the load change was very small, the deflection began to change and increase abruptly, and the specimens reached a state of destruction, in which the deflection continued to increase most obviously after RCFB1 and SRFB6 reached the ultimate load.

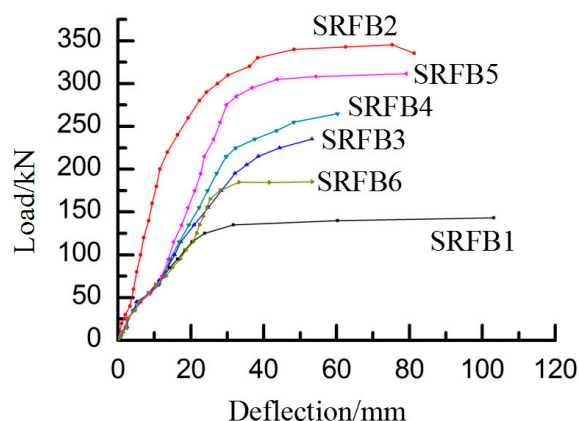


Figure 7. Load–deflection curves of the specimens.

With the increase in the secondary stress load, cracks appeared in the reactive powder concrete surface layer in the tensile zone at the bottom of the beam, the increase in the deflection was more moderate, and the slope of the load–deflection curve decreased gradually with the gradual increase in the load. Due to the bridging effect of steel fibers in the reinforcement layer, the reactive powder concrete did not stop working immediately and completely after cracking but maintained a certain ductile contribution, still possessing higher tensile strength and toughness than ordinary concrete after cracking. Thus, the slope of the curve decreased more gently than did the plastic phase deformation curve of the ordinary reinforced concrete beams, and the bending section was longer.

After the secondary stress reached the ultimate load, the width and length of the main crack in the reactive powder concrete reinforcement layer reached the maximum, the reactive powder concrete no longer bore the main stress in the tensile zone, and the longitudinal tensile reinforcement at the bottom of the beam in the reactive powder concrete reinforcement layer and in the original member reached the limit state in turn and yielded. At this time, the stiffness of the specimen rapidly decreased to failure, and the slope of the curve rapidly decreased or even increased in the reverse direction, indicating that the specimen had reached the limit of deflection and that deformation and damage had occurred. In the later stage of loading, the deflection of reinforced beams SRFB2, SRFB5, and SRFB6 increased rapidly, and after the yielding of longitudinal tensile reinforcement at the bottom of the beams, the specimens were loaded to failure due to the destruction of reactive powder concrete and concrete crushed at the top of the beams in the compression zone. The load deflection of the reinforced beams SRFB3 and SRFB4 increased rapidly, and the longitudinal reinforcement in the reinforcement layer at the bottom of the beam and the longitudinal tensile reinforcement in the original member were subsequently removed. Then, the reactive powder concrete reinforcement mesh surface layer in the pressurized zone at the top of the beam and the reinforced concrete in the original member continued to be subjected to part of the compressive stresses, the load–deflection curves entered into a transiently decreasing section, and the loads were reduced while the deflections continued to increase.

The deflection curves in Figure 8 show that the stiffness of each strengthened beam was not significantly reduced before reaching the ultimate load compared to that of the unreinforced comparison beam, and the slope of the load–angle curve was significantly greater than that of the comparison beam in the middle and late stages of the loading phase, indicating that the test beams were more ductile after load-holding reinforcement.

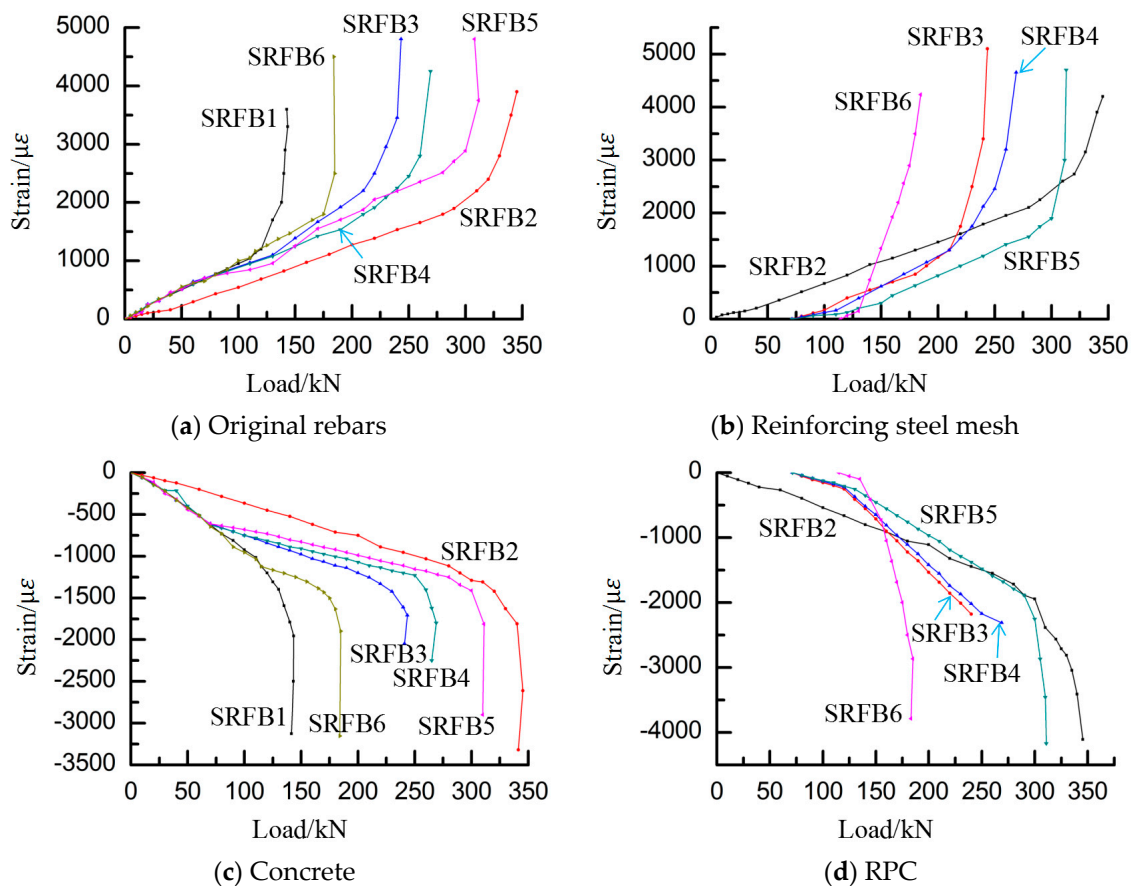


Figure 8. Strain curve in the mid-span section.

Figure 8 shows that under the condition of the same initial load-holding level, different reinforcement amounts have a significant effect on the change in longitudinal tensile reinforcement strain. For SRFB3, SRFB4, and SRFB5 in the primary loading stage, the longitudinal reinforcement strains of the bottom of the beam of the original member are the same. Due to the same initial loading level, each specimen has the same stress as the steel reinforcement of the bottom of the beam in the tensile zone of the original member when reinforced. In the second stress loading stage, the reinforcement in the reinforcement layer of each specimen is in the linear deformation stage, while the original member reinforcement strain curve re-steepens, and the reinforcement layer reinforcement strain curve changes in the same trend, indicating that the reactive powder concrete, the reinforcement layer reinforcement network, and the original member are subjected to the same force. The curve of each specimen in the late stage of the second stress loading gradually slows; the tensile deformation of the longitudinal reinforcement at the bottom of the beam in the reinforced layer and the original member is close to yielding, and the strain curve gradually becomes a gentle curve. Due to the different amounts of reinforcement in the reinforced layer at the bottom of the beam, the reinforcement layer reinforcement amount is changed, the strain curves ultimately reach different levels of loading, and the yield plateau of the largest reinforcement amount of SRFB5 is the highest. For SRFB3 with the smallest amount of reinforcement, the ultimate bearing capacity of the specimen is the lowest when the longitudinal reinforcement reaches the ultimate strain, and the ultimate strain is reached under the action of a lower load level. The yielding plateau in the ultimate strain lasts for a very short period that reaches the limit of the ultimate strain, and the ductility is not obvious in the whole process of yielding and damage. With increasing load, for the reinforced beam SRFB3 with lower reinforcement in the reinforcement layer, the reactive powder concrete in the tensile zone at the bottom of the beam exits the work earlier, the longitudinal reinforcement of the original member in the tensile zone at the

bottom of the beam and the reinforcing layer reinforcement network strains grow faster, and the tensile reinforcement quickly reaches its ultimate tensile strain. The strain curves of the reinforcement layer and original member reinforcement of each specimen show a gradual convergence trend, in which there is a strain lag and strain difference between the two in the early stage. With increasing load after the second stress, the stress level of the two gradually converges, the original member reinforcing bar strain growth is small, the reinforcement layer reinforcing bar strain growth is large, the reinforcing layer reinforcing bar greatly shares the original member reinforcing bar's stress, and the two work well. After the final curve converges, the original member longitudinal bar and reinforcement layer reinforcement network strain growth is more rapid, and the tensioned reinforcement quickly reaches its ultimate tensile strain. The final curve convergence shows that the original member and the reinforcing layer in the reinforcement have reached the yield limit, and the specimen has reached a state of destruction.

Under the condition of the same reinforcement layer reinforcement amount and different initial load-holding level conditions during secondary stressing, the difference in the strain of the longitudinal tensile reinforcement at the bottom of the specimen beams is obvious. SRFB2, SRFB5, and SRFB6 were configured with the same longitudinal tensile reinforcement at the bottom of the beams of the original members; therefore, the directions of the prestrain curves of the reinforcement were the same. Reinforcement is carried out after loading to a load level of 20% to 80% before secondary stressing, after which the reactive powder concrete, which has a lower load level, exhibits the first inflection point of the reinforcement strain curves. With the increase in the load level, the curves of SRFB5 and SRFB6 transit through the stage of linear elasticity change along the original slope, in which the slope of SRFB6, with a load level of 80%, has already begun to change, and the curves tend to be flattened, which indicates that the specimen was subjected to different degrees of plastic change in the late stage of initial stress, and some damage occurred in the bending region of the original member. After reinforcement by the reactive powder concrete reinforcing mesh reinforcement layer to share the load, the slope steepens and reverts to a linear change. The second prestress occurs over a long time in the elastic deformation stage, indicating that, at this time, the reactive powder concrete surface layer and longitudinal reinforcement in the reinforcing layer are operative and work with the original member. In the process of secondary stressing, the reinforcement in the reinforcement layer also experienced a change from elastic to final yield deformation. There is an initial strain difference between the longitudinal reinforcement in the original member and the longitudinal reinforcement in the reinforcement layer at the bottom of the beam, and the larger the initial load-holding level is, the larger the strain difference is, while the two reinforcement strain curves of the specimens finally converge, which indicates that the strain hysteresis phenomenon is gradually eliminated in the late stage of loading due to the deformation of the reinforcement in the reinforcement layer in the late stage of the secondary loading and the close to the state of the reinforcement after deformation in the primary loading. The reinforcement layer is the same as that of the original member, and damage and plastic deformation also occur. The reinforcement layer is damaged and plastically deformed, similar to the original member. In the figure, the strain difference of SRFB6 with a high initial load-holding level is the largest, which indicates that the strain hysteresis of the original member and the reinforcement layer is the most obvious. In the late loading stage, the strain curves of the longitudinal reinforcement in both the original member and the reinforced layer decrease rapidly, and the load increase is small, but the strain change is very large and rapid, indicating that the reinforcement is close to the yield state at this time. In the destructive stage after the linear elastic change in the late stage of the reinforcement, the slopes of the strain curves of the reinforcement in the reinforced layer and the reinforcement in the original member gradually decrease, the bending segment of the curves is very long, and a yielding plateau is experienced at the end. The co-stressing of the reinforced reactive powder concrete reinforcement mesh blocked the rapid yielding of the longitudinal reinforcement at the bottom of the beam of the original member, which

improved the ductility, and the effect of ductility enhancement was more obvious in SRFB6 with a higher initial load-holding level.

The compressive strain change curves of the original member concrete and reinforced reactive powder concrete in the compression zone at the top of the beam in Figure 9 show that the compressive strain values of the reinforced thin-layer reactive powder concrete are much greater than those of the original member concrete under the secondary stress state. Furthermore, the thickness of the reinforcement layer is only 25 mm, which indicates that the advantage of the ultrahigh strength of the reactive powder concrete has been fully realized. The reinforcing layers of the reinforcing beams SRFB2, SRFB5, and SRFB6 are 50×50 mm, and, in the late loading of the original component concrete and reactive powder concrete curve, the layers quickly reach the material's ultimate compressive strain, and the specimen beam top compression zone material is damaged. Moreover, at 75 mm, the compressive strain curves of the original member concrete and reactive powder concrete ranged from 2000–2500 μm ; that is, the compressive strain did not change, and the material did not reach a state of crushing. This shows that the material strength utilization efficiency of reactive powder concrete in the process of secondary force loading is different, in which the greater the amount of reinforcement in the steel reinforcement layer is, the more fully the reactive powder concrete exerts compressive strength in the compression zone.

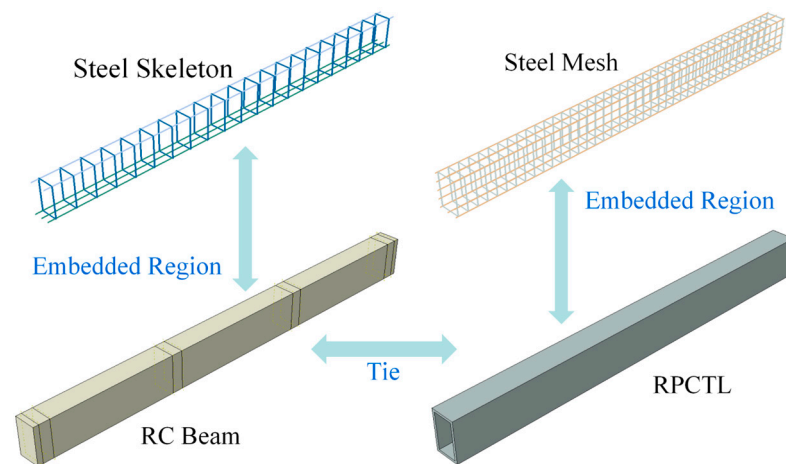


Figure 9. Numerical model assembly.

3.3. Destruction Mechanisms

The load–strain curves of the tensile reinforcement at the bottom of the concrete beams of the original members of each specimen showed two main traits: primary stress loading and secondary stressing after load-holding reinforcement. The primary stress can be subdivided into an elastic phase and a working with cracks phase, and the secondary stress can be divided into an initial elastic phase and a yield damage phase.

Before reinforcement, the original members experienced the same elastic and elastoplastic phases as did the comparison beam RCFB1, with different degrees of damage in the original members at different initial loading levels and different lengths of periods after entering the elastoplastic phase. Partial cracks appeared on the concrete surface of the original members, and the damage was more obvious in the original members with high loading loads. The cracks extended longer and wider during the elastic–plastic phase, and the stress level of the reinforcing bars in the tensile zone increased after the concrete cracked and withdrew from the work. The tensile reinforcement at the bottom of the beam was subjected to some tensile stresses and had not reached yield.

After reinforcement, the cross-section re-entered the elastic phase, and the stress strain in the cross-section at the beginning of loading was linear. The tensile stress in the tensile zone was borne by the reactive powder concrete, longitudinal reinforcement in the reinforcement layer, and longitudinal bars at the bottom of the beam of the original

member. The stress level of the longitudinal bars at the bottom of the beam of the original member was greater in the member with a higher initial loading level. The stresses shared by the reactive powder concrete at the edge of the tensile zone were greater than the tensile strength. When it exceeded its tensile strength, the surface of the reinforcement layer cracked, and the reactive powder concrete ceased to work. Subsequently, the stress in the tensile zone was mainly borne by the longitudinal reinforcement in the reinforcement layer and the longitudinal reinforcement at the bottom of the beam of the original member, and with a further increase in load, the plastic deformation of the cross-section increased, and the reinforcement layer reinforcement was close to yielding.

In the destruction stage, after the longitudinal reinforcement in the reinforcement layer at the bottom of the beam yields to tension, the plastic deformation of the section develops rapidly. The cracks continue to extend upward, and the width increases. Due to the bidirectional stress state of the reinforcing network and the bridging effect of the steel fibers, the adjacent vertical cracks are connected, the cracks bifurcate at the end, and the cracking part of the stress zone is distributed in a network with a dense and uniform distribution of cracks, in which the steel fibers in the main crack opening are pulled off. The load does not continue to increase; the longitudinal reinforcement of the reinforcement layer and original member at the bottom pull off and yield one after another, the deformation of the member continues to increase, the cross-sectional stress is redistributed, the stress in the top of the beam in the pressurized area increases rapidly, the concrete in the pressurized area collapses and deforms and expands, and the reinforced layer of reactive powder concrete crushes and spalls off.

3.4. Factor Analysis

In the test group set up for this study, the same thickness and strength level of reinforced thin-layer reactive powder concrete material were used, and the factors of variation between specimens included different reinforcement layer reinforcement amounts and initial load levels.

(1) Reinforcement layer reinforcement

Compared with that of the unreinforced comparison beam RCFB1, the initial stiffness of each reinforced beam is greater at the beginning of the secondary stress, and the slopes of the load–deflection curves of the reinforced beams SRFB5 are greater than those of SRFB4 and SRFB3 in turn with the increase in the amount of reinforcement in the reinforcing layer. This is due to the formation of small and intensive cracks in the tensile zone at the bottom of the beams after the initial cracks appear, and the presence of steel fibers that disperse the localized stresses in the material. The presence of steel fibers disperses the localized stresses in the material, resulting in a greater utilization of the strength of the reinforcing mesh material in the thin layer of reinforcement that bears the tensile action. In comparison, in the later stage of the steel yielding and concrete compression damage stage, the specimen deflection changes rapidly, the load–deflection curve is very short, and the specimen quickly enters the destruction stage and reaches the limit state. The stiffness of the reinforced beams did not decrease significantly before reaching the ultimate load, and the slope of the load–deflection curves of the reinforced beams decreased gradually but was significantly greater than that of the comparison beams in the middle and late stages of the loading phase, which indicated that the reinforced test beams had better ductility [30]. The larger the amount of reinforcement in the reinforced lamina is, the larger the ultimate load of the reinforced beam. When the reinforcing thin layer is equipped with a reinforcement mesh with a spacing of 100 mm, the load-carrying capacity of the reinforced beams is increased by 70% compared with that of the comparison beams, and the change in deflection from the point of cracking to the point of damage is 14.1 mm, whereas when the reinforcement mesh spacing is reduced to 75 and 50 mm, the increase in the ultimate load-carrying capacity is 88% and 117%, and the change in deflection is 15.2 mm and 29.0 mm, respectively. This is because the original member concrete and reinforced layer-activated powdered concrete have better ultimate loads than the reinforced layer of

active powder concrete after cracking, mainly due to longitudinal tensile reinforcement; the larger the reinforcement layer reinforcement is, the higher the late tensile strength is, and the deflection change space is also larger.

(2) Initial load level

When special cementitious materials such as composite mortar and fiber concrete are used to reinforce secondary stressed concrete members, different initial load levels have significant effects on the secondary stresses of concrete beams reinforced with cementitious materials. SRFB2, SRFB5, and SRFB6, with the same 50 mm spacing of reinforcement mesh in the reinforcement layer, reached 0%, 50%, and 80% of the ultimate capacity before reinforcement, respectively, and the load–deflection curves of these three samples basically coincided with those of comparison beam RCFB1 before reinforcement and entered the secondary stress state after the curve separation point. The later the timing of separation from the RCFB1 curve, i.e., the higher the initial load level of the reinforced beams, the shorter the growth change in the later part of the curve. With increasing load, the slope of the curve decreases gradually, in which the change in the slope of SRFB2 with the smallest initial load is the most obvious, while the change in SRFB6 with the highest initial load is very short, and the curve reaches a flat section similar to that of RCFB1 and is destroyed immediately after a very short extension. Compared with those of the comparison beams, the ultimate load-carrying capacities of SRFB2 and SRFB5 for RCFB1 increase by 141% and 117%, respectively, while that of SRFB6 improves by only 29%. SRFB2 and SRFB5, which were strengthened at lower initial load levels, showed better load capacity improvement and later stiffness performance than did RCFB1 and SRFB6, indicating that the earlier the duration of strengthening under load-holding conditions was, the greater the strengthening effect.

4. Finite Element Analysis

4.1. Model Setup

The general finite element software ABAQUS 2020 was used for finite element simulation, and each component was created and edited under the Part module (Figure 9). The original component concrete and reactive powder concrete were simulated with three-dimensional deformable solid units, and the reinforcing steel skeleton and reinforcing thin layer of the reinforcement mesh were simulated with three-dimensional deformable line units. The reinforced specimen models were generated based on the primary force to reinforce the thin layer, and then the secondary force holding load loading was realized through the method of living and dead cells. In the model, the concrete grid size of the original member was 50 mm, the grid size of the reinforcing skeleton of the original member was 50 mm, the cell size in the thickness direction of the reinforced thin layer of reactive powder concrete was 25 mm, and the cell size in the plane direction of the thin layer was 50 mm. The contact between the reinforcing mesh and the reactive powder concrete, as well as the contact between the reinforcing skeleton of the original member and the concrete, were all constrained using embedded constraints, and there was no interfacial slippage in the process of stress [31]. Memduh Karalar carried out a numerical investigation on the flexural response, and especially the crack failure, of rubberized concrete beams reinforced by waste tire rubber and plastic waste [32,33], where the boundary condition of no slip was set between the reinforced layer and the original member. Memduh Karalar used three-dimensional finite element mode shapes to study the flexural performance of concrete beams doped with WTR by defining the beam members as nonlinear frames, which provides a reference for the finite element analysis of the same type of composite-reinforced beams [34]. Tie constraints were used for the contact relationship between the RPC and concrete. Line constraints were used to simulate the boundary conditions [4], and the support constraints were set on the original concrete beams. One end was supported on a fixed hinge bearing, and one end was supported on a movable hinge bearing. The fixed-hinge constraints D_x , D_y , and D_z were all set to 0. The sliding-hinge constraints D_x and D_y were set to 0, but the displacement in the Z direction was not constrained.

4.2. Comparison of Results

The numerical simulation results of the ultimate bearing capacity and maximum deflection are shown in Figure 10, and the comparison results show that the ratio of the test value to the simulated value of the ultimate bearing capacity of each specimen ranges between 0.927 and 1.087, and the ratio of the test values to the simulated values of the displacement ranges between 0.921 and 1.090, which is in good agreement with the test results.

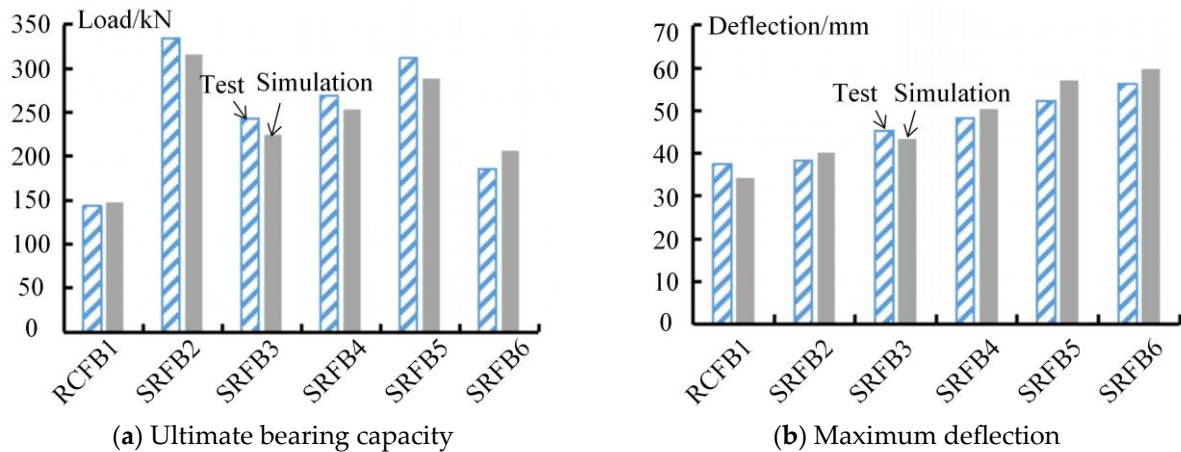


Figure 10. Comparison of the numerical analysis and test-results.

4.3. Strain and Cracks

The results of the damage simulation of the reinforced thin layer of reactive powder concrete are shown in Figure 11, in which the crushed area between the two loading points in the damage cloud map is mainly concentrated in the loading point area, while the observed morphology in the experimental phenomenon is mainly in the mid-span region in the middle of the loading point. This is because the numerical simulation does not consider the case in which the two loading points are rigidly connected through the distributing beams, and the localized peeling of the reinforced thin layer during the crushing damage on the top of the beams at the later stage of the actual loading varies with the tie constraints of the numerical simulation.

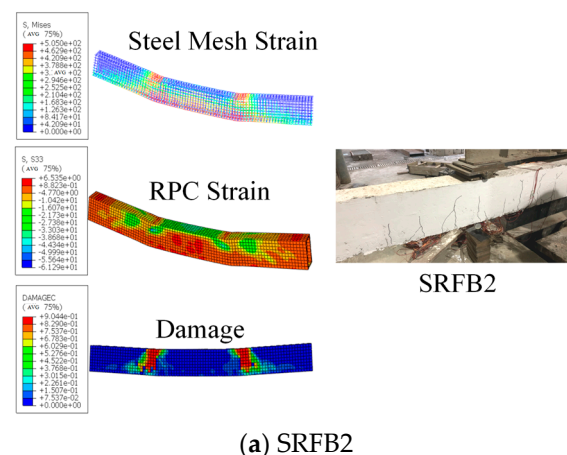


Figure 11. Cont.

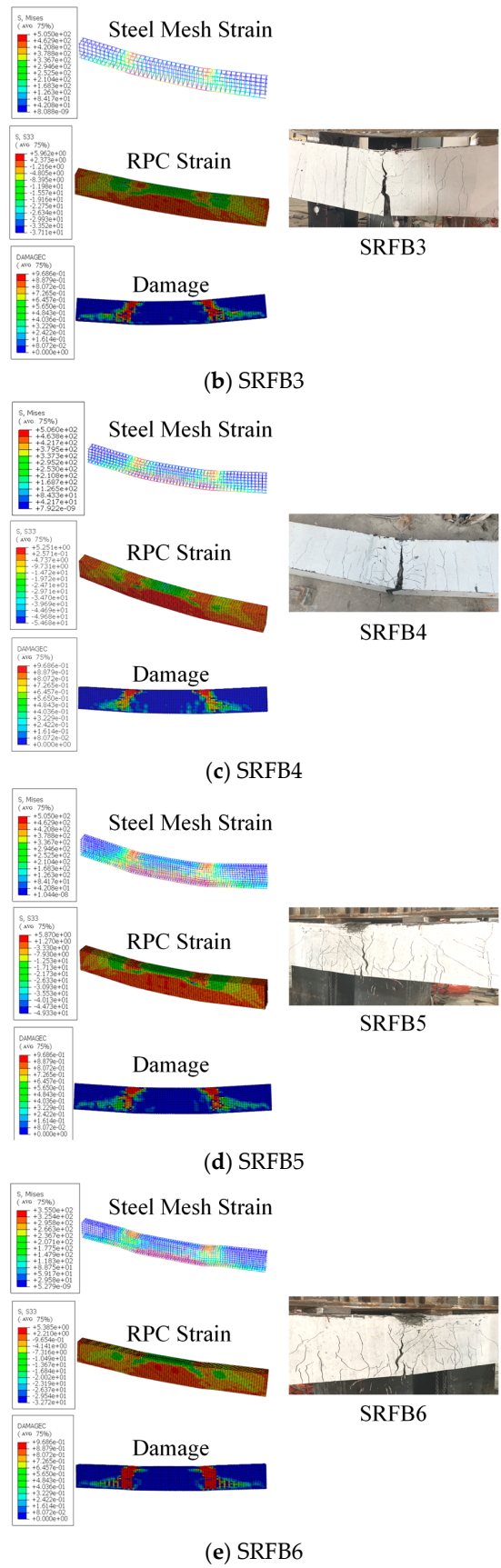


Figure 11. Simulation results of stress and damage.

5. Calculation of the Reinforcement Load Capacity

In the test and simulation analysis, the thin layer of reactive powder concrete on the top surface of the beam in the compression zone also reaches the ultimate compressive strain, while the side of the beam from the top to the bottom in the height range is similar to that of the concrete and is not linearly distributed. Therefore, the calculation of the compression zone of the reactive powder concrete is divided into two parts for consideration. The thin layer on the top surface of the beam is directly treated according to the strain reaching the peak strain, and the strain after reaching the peak strain is considered to remain unchanged. The active powder concrete in the height range of the compression zone in the reinforcement layer on the side of the beam is transformed into an equivalent rectangular section in the same way as the concrete in the compression zone.

When performing flexural reinforcement calculations, the beam top surface and beam side reinforcement network in the compression zone are not considered, while the top surface of the beam in the compression zone and the beam side reactive powder concrete under compression are considered. Under the limit state, the longitudinal reinforcement at the bottom of the beam yields, and the concrete at the edge of the top of the beam in the pressurized zone is damaged; the force diagram of the reinforced member is shown in Figure 12. The bending capacity of the reinforced beam consists of the following parts: the tensile action of the longitudinal bars at the bottom of the original member, the tensile longitudinal bars at the bottom of the beam reinforcement layer, the tensile longitudinal bars at the side of the beam reinforcement layer, the compressive action of the longitudinal bars at the top of the original member, the concrete in the height range of the top compression zone of the beam, and the activated powdered concrete. According to the assumption of a flat section and the condition of force equilibrium within the section, the moment of any section within the section is zero.

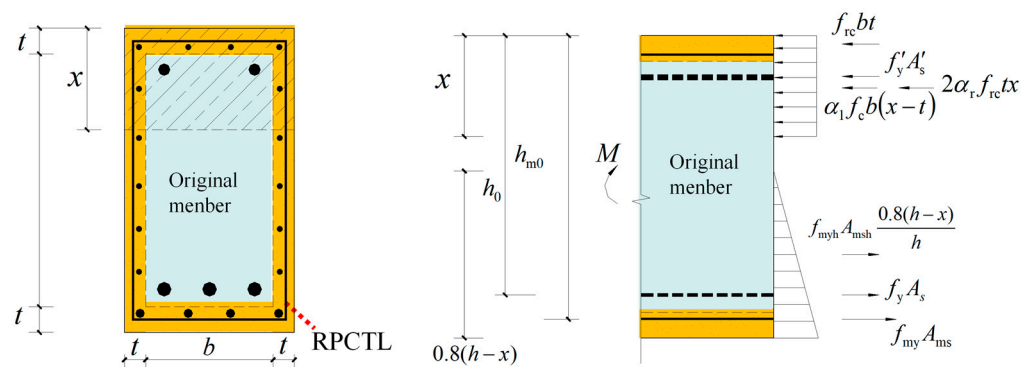


Figure 12. Schematic diagram for calculating the flexural load capacity.

5.1. Height of the Reinforced Compression Zone

The compressive stresses of concrete above the neutralization axis and reactive powder concrete are nonlinearly distributed in the height range of the compression zone, which is transformed into an equivalent rectangle by coefficients in most of the research; the coefficients of concrete (α_1) are 0.94~1.0 in GB50010-2010 [35], the coefficients of reactivated concrete (α_r) are 0.95 in T/CECS1325-2023 [36], and the coefficient of RPC100 adopted in this paper is 0.95.

According to the force equilibrium condition shown in Figure 12.

$$f_y A_s + f_{my} A_{ms} + 2f_{myh} \frac{0.8(h-x)}{h} A_{msh} = \alpha_1 f_c b (x-t) + 2\alpha_r f_{rc} t x + f_{rc} t b + f'_y A'_s \quad (1)$$

$$x = \frac{f_y A_s + f_{my} A_{ms} + 1.6f_{myh} A_{msh} + \alpha_1 f_c b t - f_{rc} t b - f'_y A'_s}{\alpha_1 f_c b + 2\alpha_r f_{rc} t + 1.6f_{myh} A_{msh}/h} \quad (2)$$

where x' is the height of the reinforced compression zone; t is the thickness of the reinforced lamina; f_{my} and f_{myh} are the tensile strengths of the reinforced layer tensile longitudinal bars at the bottom and side of the beam, respectively; A_{ms} and A_{msh} are the areas of the reinforced layer tensile longitudinal bars at the bottom and side of the beam, respectively; and f'_y and A'_s are the compressive strengths of the reinforced compression reinforcement at the top of the reinforced beam and the area of the reinforced compression reinforcement, respectively.

5.2. Conversion of the Cross-Sectional Area of the Tensile Reinforcement

Considering that the side of the beam is subjected to tensile stress only within a certain height, the cross-sectional area reduction coefficient of the reinforcement is introduced to reduce the cross-sectional area of the longitudinal reinforcement, providing tensile stress in the thin layer of the beam side reinforcement [23]. According to the cross-sectional results of the ECC- and HDC-reinforced concrete beams, this coefficient is 0.8, and the longitudinal reinforcement in the thin layer of the beam side reinforcement does not reach the yielding of the longitudinal bars in its entirety. Therefore, the stress distribution of the tensile longitudinal reinforcement in the thin layer of the beam side reinforcement is regarded as a triangle with a linear change along the direction of the beam height and a height of $0.8(h - x)$, which reaches yielding near the bottom of the beam and is 0 near the side of the neutralization axis, and the point of the combined force is located in the center of the triangle at a distance of $0.8(h - x)/3$ from the bottom of the beam. The height of the compression zone of the reinforced specimen x can be solved according to the cross-sectional force balance equation, in which the combined force of the concrete in the compression zone and the active powder concrete in the reinforced lamina on the side of the beam in the compression zone is equal to the combined force of the original longitudinal reinforcement at the bottom of the beam, the longitudinal reinforcement in the reinforced lamina at the bottom of the beam, and the longitudinal reinforcement in the reinforced lamina on the side of the beam in the range of the height of the beam at the bottom of the beam $0.8(h - x)$. The bending capacity of RPCTL-reinforced RC beams can be expressed as follows:

$$M \leq f_y A_s \left(h_0 - \frac{x}{2} \right) + f_{my} A_{ms} \left(h_{m0} - \frac{x}{2} \right) + \frac{1.6(h - x)}{h} f_{myh} A_{msh} \frac{0.8(h - x)}{3} \quad (3)$$

The calculation results of specimens under the same load-holding conditions obtained by using the above formula are shown in Table 8, and the test results are consistent with the calculation results. The results show that the calculation results of the formula derived in this paper for the bending capacity of RPCTL-reinforced RC beams are highly accurate and can be used in the reinforcement design of similar concrete beams.

Table 8. Calculation results and comparison.

Specimen	Test Results (kN)	Calculation Results (kN)	Ratio
SRFB3	243.5	250.8	0.971
SRFB4	269.5	282.2	0.955
SRFB5	311.5	324.3	0.961

6. Conclusions

- (1) The application of four-sided RPCTL reinforcement technology can effectively improve the bending load capacity and stiffness of concrete beams; the specimen cracking load is greatly increased by 1.42 times to 7.12 times, the ultimate bearing capacity is increased by 0.29 times to 1.41 times, and the deflection and deformation are effectively controlled.

- (2) Four-sided reinforcement significantly suppresses cracking in reinforced concrete flexural beams. As longitudinal tensile reinforcement yields, the top zone experiences compression dominated by crushing. This leads to crack openings, causing steel fibers to slip and pull out, while the reactive powder concrete substrate surface in the compression zone is crushed, fractured, and spalled.
- (3) Increasing the amount of reinforcement in the reinforced thin layer and appropriately reducing the initial load level before secondary stressing can improve the effectiveness of four-sided RPCTL reinforcement.
- (4) The results of the dynamic numerical simulation and analysis of the RPCTL reinforcement test process show that the test results are in good agreement with the simulation results of the numerical analysis, with the ratio of the ultimate bearing capacity ranging from 0.927 to 1.087 and the ratio of the displacement deflection ranging from 0.921 to 1.090.
- (5) A method for calculating the bending capacity of four-surface RPCTL-reinforced concrete beams is proposed, where the load-carrying capacity of the reinforced member consists of three parts: the load-carrying capacity provided by the original member itself, the tensile load-carrying capacity provided by the reinforcing layer of the reinforcement mesh, and the compressive load-carrying capacity provided by the reactive powder concrete surface layer. The calculated results are in good agreement with the test values, which can be used in the reinforcement design of similar concrete beams.

Author Contributions: Conceptualization, W.L. and W.Y.; methodology, W.L.; software, W.L.; validation, W.L. and W.Y.; formal analysis, W.L.; investigation, W.Y.; resources, W.L. and J.Y.; data curation, W.L.; writing—original draft preparation, W.L.; writing—review and editing, W.L. and W.Y.; visualization, W.L.; supervision, W.Y.; project administration, W.Y. and W.L.; validation, J.Y.; funding acquisition, J.Y. All authors have read and agreed to the published version of the manuscript.

Funding: This research was funded by the Hunan Natural Science Foundation, grant number 2023JJ30045.

Data Availability Statement: The original contributions presented in the study are included in the article material, and further queries can be directed to the corresponding author.

Conflicts of Interest: The authors declare no conflicts of interest.

References

1. Azeez, A.A.; Jaafar, A.A.; Yussof, M.M.; Blash, A.A.A. Study of the Behavior of Reactive Powder Concrete RC Deep Beams by Strengthening Shear Using Near-Surface Mounted CFRP Bars. *Open Eng.* **2023**, *13*, 20220433. [[CrossRef](#)]
2. Zhelyazov, T.; Thorhallsson, E. Analytical and Numerical Approaches for the Design of Concrete Structural Elements with Internal BFRP Reinforcement. *Materials* **2022**, *15*, 1497. [[CrossRef](#)]
3. Codina, A.; Barris, C.; Jahani, Y.; Baena, M.; Torres, L. Assessment of Fib Bulletin 90 Design Provisions for Intermediate Crack Debonding in Flexural Concrete Elements Strengthened with Externally Bonded FRP. *Polymers* **2023**, *15*, 769. [[CrossRef](#)]
4. Gedik, Y.H.; Betschoga, C.; Tung, N.D.; Tue, N.V. Numerical Investigation on the Shear Behavior of Slender Reinforced Concrete Beams without Shear Reinforcement Differed by Various Boundary and Loading Conditions. *Structures* **2023**, *50*, 870–883. [[CrossRef](#)]
5. de Sousa Leite, L.; Souza, M.T.; da Silva, E.J.; Benvenuti, T.; de Castro Pessôa, J.R.; Amado, F.D.R. Assessing the Flexural Strength of Reinforced Concrete Beams with Bamboo Splints Co-Assembled to Steel Rebars under Three- and Four-Point Flexural Strength Testing. *Case Stud. Constr. Mater.* **2024**, *20*, e02933. [[CrossRef](#)]
6. Karalar, M.; Özkılıç, Y.O.; Deifalla, A.F.; Aksoylu, C.; Arslan, M.H.; Ahmad, M.; Sabri, M.M.S. Improvement in Bending Performance of Reinforced Concrete Beams Produced with Waste Lathe Scraps. *Sustainability* **2022**, *14*, 12660. [[CrossRef](#)]
7. Njeem, W.; Aoude, H.; Martín-Pérez, B.; Jade, A. Blast Performance and Analysis of Reinforced Concrete Beams Subjected to Corrosion of the Longitudinal Reinforcement. *Struct. Concr.* **2023**, *24*, 239–256. [[CrossRef](#)]
8. Samarakoon, S.M.S.M.K.; Piatek, B.; De Silva, G.H.M.J.S. Investigation of the Flexural Behavior of Preloaded and Pre-Cracked Reinforced Concrete Beams Strengthened with CFRP Plates. *Materials* **2023**, *16*, 22. [[CrossRef](#)]
9. Wang, X.; Liu, S.; Shi, Y.; Wu, Z.; He, W. Integrated High-Performance Concrete Beams Reinforced with Hybrid BFRP and Steel Bars. *J. Struct. Eng.* **2022**, *148*, 04021235. [[CrossRef](#)]
10. Xin, Q.; Niu, Q.; Zhang, M.; Li, Z.; Gao, R. Effect of Chlorine Salt Erosion on Flexural Performance of GFRP and Steel Bars Hybrid Reinforced Beams. *Structures* **2024**, *59*, 105779. [[CrossRef](#)]

11. Wang, Z.; Wang, Q.F.; Zhang, L. Research on the Influence of the Steel Fiber on RPC Performance. *Adv. Mater. Res.* **2014**, *1065–1069*, 1833–1837. [[CrossRef](#)]
12. Wang, C.; Xue, G.; Zhao, X. Influence of Fiber Shape and Volume Content on the Performance of Reactive Powder Concrete (RPC). *Buildings* **2021**, *11*, 286. [[CrossRef](#)]
13. Rong, Q.; Zhao, Z.; Hou, X.; Jiang, Z. A P-I Diagram Approach for Predicting Dynamic Response and Damage Assessment of Reactive Power Concrete Columns Subjected to Blast Loading. *Buildings* **2022**, *12*, 462. [[CrossRef](#)]
14. Liu, M.; Dai, W.; Zhong, C.; Yang, X. Study on Mechanical Properties and Microstructure of Basalt Fiber Reactive Powder Concrete. *Buildings* **2022**, *12*, 1734. [[CrossRef](#)]
15. Mohammed, S.D.; Ibrahim, T.H.; Salman, B.F.; Allawi, A.A.; El-Zohairy, A. Structural Behavior of Reactive Powder Concrete under Harmonic Loading. *Buildings* **2023**, *13*, 1917. [[CrossRef](#)]
16. Xiao, J.; Murong, Y.; Chen, X.; Liu, L.; Zhai, K.; Jiang, H.; Huang, L.; Wang, G. Research on the Bonding Performance of BFRP Bars with Reactive Powder Concrete. *Buildings* **2023**, *13*, 2083. [[CrossRef](#)]
17. Lee, M.-G.; Huang, Y.S.; Kan, Y.C.; Wang, W.C.; Wang, Y.C.; Wu, C.H. Flexure Strengthening and Analysis Using CFRP Composite and Reactive Powder Concrete. *Buildings* **2023**, *13*, 1890. [[CrossRef](#)]
18. Yang, Y.; Xu, C.; Yang, J.; Wang, K. Experimental Study on Flexural Behavior of Precast Hybrid UHPC-NSC Beams. *J. Build. Eng.* **2023**, *70*, 106354. [[CrossRef](#)]
19. Yang, K.; Su, H.; Dai, T.; Li, K.; Lin, Y. Experimental Study on the Flexural Tensile Properties of Aligned Steel Fiber-Reinforced Reactive Powder Concrete Members. *Struct. Concr.* **2023**, *24*, 1486–1502. [[CrossRef](#)]
20. Zhang, Y.; Li, X.; Zhu, Y.; Shao, X. Experimental Study on Flexural Behavior of Damaged Reinforced Concrete (RC) Beam Strengthened by Toughness-Improved Ultra-High Performance Concrete (UHPC) Layer. *Compos. B Eng.* **2020**, *186*, 107834. [[CrossRef](#)]
21. Zhang, Y.; Huang, S.; Zhu, Y.; Hussein, H.H.; Shao, X. Experimental Validation of Damaged Reinforced Concrete Beam Strengthened by Pretensioned Prestressed Ultra-High-Performance Concrete Layer. *Eng. Struct.* **2022**, *260*, 114251. [[CrossRef](#)]
22. Bahraq, A.A.; Al-Osta, M.A.; Ahmad, S.; Al-Zahrani, M.M.; Al-Dulaijan, S.O.; Rahman, M.K. Experimental and Numerical Investigation of Shear Behavior of RC Beams Strengthened by Ultra-High Performance Concrete. *Int. J. Concr. Struct. Mater.* **2019**, *13*, 6. [[CrossRef](#)]
23. Deng, M.; Ma, F.; Ye, W.; Li, F. Flexural Behavior of Reinforced Concrete Beams Strengthened by HDC and RPC. *Constr. Build. Mater.* **2018**, *188*, 995–1006. [[CrossRef](#)]
24. Farzad, M.; Shafieifar, M.; Azizinamini, A. Experimental and Numerical Study on Bond Strength between Conventional Concrete and Ultra High-Performance Concrete (UHPC). *Eng. Struct.* **2019**, *186*, 297–305. [[CrossRef](#)]
25. Zhu, Z.; Abdelbaset, H.; Li, X.; Tang, Q. Flexural Behavior of Long-Term Loaded RC Beams Strengthened by Ultra-High Performance Concrete. *Constr. Build. Mater.* **2023**, *407*, 133428. [[CrossRef](#)]
26. Qin, F.; Zhang, Z.; Yin, Z.; Di, J.; Xu, L.; Xu, X. Use of High Strength, High Ductility Engineered Cementitious Composites (ECC) to Enhance the Flexural Performance of Reinforced Concrete Beams. *J. Build. Eng.* **2020**, *32*, 101746. [[CrossRef](#)]
27. Yi, T.; Wang, H.; Xie, J.; Wang, W. Flexural Strength and Acoustic Damage Characteristics of Steel Bar Reactive Powder Concrete. *Appl. Sci.* **2021**, *11*, 7017. [[CrossRef](#)]
28. Xu, X.; Li, Y.; Yu, B.; Zhu, B.; Liu, Q.; Hu, H.; Hu, Z.; Yu, B.; Wang, S.; Meng, J. A Novelty Method of Multi-Scale Toughening Cement-Based Materials: Reactive Powder Concrete with Endogenous Whiskers. *J. Build. Eng.* **2022**, *50*, 104142. [[CrossRef](#)]
29. Elsayed, M.; Badawy, S.; Tayeh, B.A.; Elymany, M.; Salem, M.; ElGawady, M. Shear Behaviour of Ultra-High Performance Concrete Beams with Openings. *Structures* **2022**, *43*, 546–558. [[CrossRef](#)]
30. Tulonen, J.; Laaksonen, A. Variable Compression Panel Thickness for Concrete Members under Bending and Torsion: Experimental Study. *Eng. Struct.* **2023**, *279*, 115606. [[CrossRef](#)]
31. Yang, J.; Wang, L.; Yang, D.; Wang, Q. Influence of Concrete and Unbonded Ratio on RC Beams. *Constr. Build. Mater.* **2023**, *403*, 133086. [[CrossRef](#)]
32. Korkut, F.; Karalar, M. Investigational and Numerical Examination on Bending Response of Reinforced Rubberized Concrete Beams Including Plastic Waste. *Materials* **2023**, *16*, 5538. [[CrossRef](#)]
33. Karalar, M. Experimental and Numerical Investigation on Flexural and Crack Failure of Reinforced Concrete Beams with Bottom Ash and Fly Ash. *Iran. J. Sci. Technol. Trans. Civ. Eng.* **2020**, *44*, 331–354. [[CrossRef](#)]
34. Karalar, M.; Ozturk, H.; Ozkilic, Y.O. Yasin Onuralp Ozkilic. Experimental and numerical investigation on flexural response of reinforced rubberized concrete beams using waste tire rubber. *Steel Compos. Struct.* **2023**, *48*, 43–57. [[CrossRef](#)]
35. GB/T 50010-2010; Code for Design of Concrete Structures. Standards Press of China: Beijing, China, 2015.
36. T/CECS1325-2023; Technical Specification for Strengthening Concrete structure with Thin Layer of High Strength Steelmesh and Reactive Powder Concrete. China Planning Press: Beijing, China, 2023.

Disclaimer/Publisher’s Note: The statements, opinions and data contained in all publications are solely those of the individual author(s) and contributor(s) and not of MDPI and/or the editor(s). MDPI and/or the editor(s) disclaim responsibility for any injury to people or property resulting from any ideas, methods, instructions or products referred to in the content.